Experimental and numerical analysis for high intensity swirl based ultra-low emission flameless combustor operating with liquid fuels

V. Mahendra Reddy [a,b], Amit Katoch [a], William L. Roberts [b], Sudarshan Kumar [a,*]

[a] *Department of Aerospace Engineering, Indian Institute of Technology Bombay, Powai, Mumbai 400 076, India*
[b] *Clean Combustion Research Center, King Abdullah University of Science and Technology (KAUST), Thuwal 23955, Saudi Arabia*

Available online 21 June 2014

Abstract

Flameless combustion offers many advantages over conventional combustion, particularly uniform temperature distribution and lower emissions. In this paper, a new strategy is proposed and adopted to scale up a burner operating in flameless combustion mode from a heat release density of 5.4–21 MW/m^3 (thermal input 21.5–84.7 kW) with kerosene fuel. A swirl flow based configuration was adopted for air injection and pressure swirl type nozzle with an SMD 35–37 μm was used to inject the fuel. Initially, flameless combustion was stabilized for a thermal input of 21.5 kW ($\dot{Q}'''$=5.37 MW/m^3). Attempts were made to scale this combustor to higher intensities *i.e.* 10.2, 16.3 and 21.1 MW/m^3. However, an increase in fuel flow rate led to incomplete combustion and accumulation of unburned fuel in the combustor. Two major difficulties were identified as possible reasons for unsustainable flameless combustion at the higher intensities. (i) A constant spray cone angle and SMD increases the droplet number density. (ii) Reactants dilution ratio (R_{dil}) decreased with increased thermal input. To solve these issues, a modified combustor configuration, aided by numerical computations was adopted, providing a chamfer near the outlet to increase the R_{dil}. Detailed experimental investigations showed that flameless combustion mode was achieved at high intensities with an evenly distributed reaction zone and temperature in the combustor at all heat intensities. The emissions of CO, NO$_x$ and HC for all heat intensities ($\Phi = 1$–0.6) varied between 11–41, 6–19 and 0–9 ppm, respectively. These emissions are well within the range of emissions from other flameless combustion systems reported in the literature. The acoustic emission levels were also observed to be reduced by 8–9 dB at all conditions.
© 2014 The Combustion Institute. Published by Elsevier Inc. All rights reserved.

Keywords: Flameless combustion; Swirl flow combustion; Liquid fuel; High intensity; Burner scaling

* Corresponding author. Address: Combustion Research Laboratory, Department of Aerospace Engineering, Indian Institute of Technology Bombay, Mumbai 400 076, India. Fax: +91 22 2572 2602.
   E-mail address: sudar@aero.iitb.ac.in (S. Kumar).

1. Introduction

Flameless/Mild combustion has gained significant importance due to its ability to suppress thermal NO formation and improve thermal efficiency

of combustion systems. Flameless combustion has been primarily identified with gaseous fuels and extensive work has been reported [1–10]. Scaling the flameless combustors to higher intensities has been proposed in recent studies reported in the literature [7,8,11]. A brief summary of various high intensity flameless combustion systems with gaseous fuels is listed in Table 1. Lückerath et al. [11] have developed a Forward Flow (FF) combustor configuration with a thermal input of 475 kW and heat intensity of 240 MW/m³ (at 20 bar). Kumar et al. [7] have scaled up a high-intensity combustor (5–150 kW thermal input) with new scaling methodology and compared various existing scaling techniques *i.e.* Constant Velocity (CV), Constant Residence Time (CRT) and Cole's approach with the proposed technique. The comparison of Weber [12] shows that CRT approach is relatively better for scaling swirl type combustor configurations. They have hinted at the need of maintaining high reactant dilution rates to ensure that flameless combustion mode is achieved in scaled combustors. These types of combustor configurations with high heat intensity are expected to be useful in gas-turbine applications. Arghode and Gupta [8] have demonstrated a laboratory scale combustor achieving colorless distributed combustion with a high intensity of 453 MW/m³ ($Q_{th} = 6.25$ kW) with a combustor volume of ~13 cm³ and Reverse Flow (RF) configuration. Scaling of these concepts with low thermal input and high heat intensity render the systems very complex and making their implementation highly challenging. Further, very little literature is available in the field of scaling of flameless combustors with liquid fuels. Some basic studies on flameless/mild combustion with liquid fuels [3,5,13–15] have been reported recently. Traditional industrial burners and stationary gas-turbine combustors operate with liquid fuels at higher thermal inputs (~1 MW) and higher heat intensities (100 MW/m³). Therefore,

additional studies are required to investigate the issues related to the scaling of high intensity flameless combustors with liquid fuels and their relation with spray characteristics.

In this study, a swirl based combustor operating in flameless combustion mode with kerosene at 21.5 kW (base case, $\dot{Q}''' = 5.37$ MW/m³) [16], is developed and scaled up to operate at 85 kW (21.1 MW/m³). Attempts were made to achieve flameless combustion with higher intensity of 10.2, 16.3 and 21.1 MW/m³ using the base case combustor configuration with increased thermal input of 40.8, 65.1 and 84.7 kW respectively. However, the existing combustor configuration was unable to achieve stable flameless combustion. Computational and experimental studies were carried out to identify the causes preventing successful scale-up of the combustor. The combustor configuration was modified by providing a chamfer, thus increasing the degree of recirculation in the combustor, allowing stable flameless combustion. Computational studies show that with increased chamfer radius (R_C), recirculation of the combustion products and fuel residence time increased. Three different R_C values were considered, for the 10.2, 16.3 and 21.1 MW/m³ cases respectively, and shown to achieve combustion with low emissions. The influence of spray characteristics on scaling the combustor was studied and the results are presented in this paper.

2. Computational studies

2.1. Geometry design methodology

The base combustor was designed to stabilize high intensity flameless combustion using conventional liquid fuels. Stabilization of flameless combustion with liquid fuels depends on three important parameters,

1. Sauter Mean Diameter (SMD) of the spray. The evaporation rate is a function of boiling point and surface area to volume ratio (A_S/V) of the droplet. The evaporation time increases with increasing boiling temperature and SMD.
2. A group of parameters including droplet distribution, evaporation, mixture formation and subsequent combustion with preheating and dilution of reactants.
3. In flameless combustion mode, the increased dilution of fresh reactants with hot combustion products results in reduced reaction rate. Due to this, reaction zone is uniformly distributed throughout the combustor volume with lower peak flame temperature than that of conventional mode [4]. In conventional mode, the fuel spray directly enters the combustion

Table 1
Variation of heat intensities reported in literature (SJ: Straight Jet, Forward Flow, FF (*i.e.* reactants enters from one side and products leave from opposite side), Reverse Flow, RF (*i.e.* reactants and products from same side of the combustor), Q_{th}: Thermal input (kW) and $\dot{Q}'''$: Heat intensity (MW/m³), S: Solid, L: Liquid, G: Gas.

Refs.	Q_{th}	$\dot{Q}'''$	Fuel	Remarks
[2]	5	10	G	SJ, FF
[3]	580	0.024	G,L,S	SJ, RF
[5]	0.4	0.58	G, L	SJ, RF
[6]	20	0.44	G	SJ, RF
[7]	150	5.6	G	SJ, FF
[8]	6.25	453	G	SJ, RF
[9]	15	0.3	G	SJ, RF
[11]	474	240	G	SJ, FF

zone having higher peak temperature. Therefore, the droplet evaporation rate is relatively slower in flameless combustion mode [4]. To achieve complete evaporation and combustion, the droplet residence time should be higher in flameless combustion mode.

To sustain flameless combustion with liquid fuels, the above three issues can be addressed by increasing the residence times and recirculation as compared to flameless combustion with gaseous fuel. A swirl flow creates a central vortex zone and low pressure gradient, supporting a large reverse flow region in the combustor. High swirl creates higher centrifugal force that enhances the residence time of the hot gases trapped within the swirling flow [13–20]. The increased residence time enhances the flame stability limits and rate of mixing of products and reactants. The high recirculation allows for good mixing, essential for obtaining a distributed reaction zone over a large volume of the combustor [13–20]. Therefore, a tangential air injection scheme was used in this study to generate the swirl flow in the combustor.

In this study, a conical combustor with 60° diverging angle was considered with a total volume of ~0.004 m^3 [16,21]. A pressure swirl fuel injector was used for injection of kerosene. The combustor configuration is shown in Fig. 1. Computational and experimental studies were carried out simultaneously. Recirculation of combustion products was identified as the key factor to sustain flameless combustion. Hence, the reactants dilution ratio (R_{dil}) is the governing metric. R_{dil} is calculated as follows [14,16].

$$R_{dil} = \frac{\dot{m}_{axial} - (\dot{m}_{ox} + \dot{f})}{(\dot{m}_{ox} + \dot{m}_f)}$$

$$\dot{m}_{axial} = \rho v_{axial} dy dz$$

2.1.1. Challenges in scaling

Initially, the combustor was tested at 21.5 kW thermal input using the unmodified combustor configuration (without chamfer, i.e. $R_C = 0$ mm) and exit diameter (D) of 25 mm. Well stabilized flameless combustion was observed experimentally [16,21]. Computational results showed that R_{dil} varied spatially from 1.1 to 3.2. The same combustor was tested at higher thermal inputs of 40.8, 65.1 and 84.7 kW (respective heat intensities 10.2, 16.3 and 21.1 MW/m^3) and experimental observations revealed that, flameless combustion was not stabilized in the combustor at these higher inputs and large quantities of unburned fuel accumulated in the combustor. The fuel spray cone angle was maintained constant at 45° for all nozzles and SMD of all nozzles were in the range of 35–37 μm (details in Section 4.1). Therefore, with the increased fuel mass flow rate, droplet number
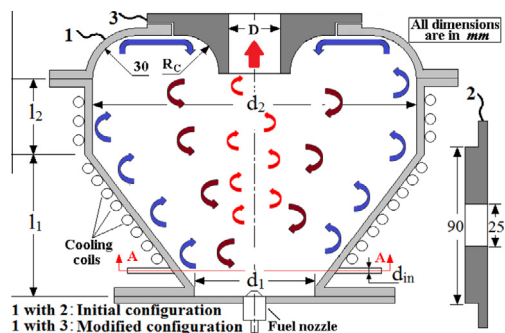

Fig. 1. Dimensional details of the combustor.

density (DND) also increased. Hence, more recirculation (increased residence time) would be required to increase the entrainment and to achieve complete evaporation. The computational results also revealed that, R_{dil} decreased with increasing thermal input. Computational and experimental evidence suggested that R_{dil} needed to be sufficiently high for all thermal inputs to provide the required entrainment and residence time.

CRT approach appears suitable for scaling swirl combustors operating with gaseous fuels [12]. However in case of liquid fuels, the DND increases with thermal input. The residence time should be increased for complete evaporation and combustion. CV scaling approach for higher thermal inputs results in increased combustor volume and reduced heat intensity [7,12]. Hence, for the present case, both CV and CRT approaches are not suitable. Similarity of certain dimensionless quantities in scaling is different for various combustor configurations, operating conditions and modes of combustion [22]. Therefore, a combination of experimental and numerical simulations aimed at improving the droplet residence times and recirculation rates were considered. To enhance both droplet residence time and recirculation rate, a chamfer at the top of the combustor is provided as shown in Fig 1. A computational analysis (described below) was carried out for high thermal inputs, by varying chamfer radius (R_C) to determine the R_{dil} for each case and the operating conditions that yielded an $R_{dil} > 2.5$. The combustor geometry for different thermal intensities is non-dimensionalized with D, as shown in Fig. 1 and listed in Table 2.

2.1.2. Numerical method

A general purpose CFD code Fluent-14.5 was used for computational studies in this work. A 3-D double-precision pressure-based solver was used. For all thermal inputs, tangential air inlet and combustor exit velocities were maintained constant to ensure similar level of pressure drop across the combustor. Therefore, the air inlet diameter (d_{in}) and exit diameter (D) are increased

Table 2
Dimensional details of the combustor.

Q_{th}	$\dot{Q}'''$	d	D	d_1	d_2	l_1	l_2	R_c	d_{in}
21.5	5.37	5	25	3.2	8.4	4.4	2.4	0.4	0.2
40.8	10.2	7.5	29	2.758	7.241	3.793	2.068	0.689	0.258
65.1	16.3	9	34	2.325	6.176	3.235	1.764	0.735	0.264
84.7	21.1	11	37	2.162	5.675	2.972	1.621	0.81	0.297

with increased thermal input. Chamfer radius is varied from 10 to 30 mm at 5 mm increments.

Three-dimensional Navier–Stokes equations were discretized and solved in a finite-volume domain. Reynolds Stress Model (RSM) was used for turbulence modeling. The energy equation was solved considering 20 intermediate species equilibrium chemistry and a non-premixed droplet combustion model for simulating the combustion of the liquid fuels. Compressible flow was considered and the viscosity was calculated using Sutherland's law. Specific heats were defined as a function of the temperature (piecewise-polynomial). A P1 radiation model was used. Constant mass-flow inlet condition normal to the boundary surface was applied at air inlets, and a pressure outlet based boundary condition was applied at the exit. No-slip wall and constant temperature boundary conditions were applied at the walls. Non-premixed droplet evaporation and combustion, following the spherical law was considered with PDF droplet evaporation. A single component surrogate, $C_{12}H_{23}$ was used to simulate kerosene with a density of 780 kg/m³ Fuel injection was simulated as a solid cone type spray with a droplet diameter of 36 μm and a cone angle of 45°. The amount of heat removal from the combustor walls is 3.2, 8.3, and 12.9 kW respectively, for three higher heat intensities of 10.2, 16.3 and 21.1 MW/m³. The heat removal through wall cooling is considered by applying heat-loss through combustor walls as heat flux boundary condition for higher heat intensity cases. The solution is considered to be converged when RMS residuals of the system were less than 1×10^{-6}. A number of computations were carried out using hexa mesh with different mesh sizes varying from 1.1 to 2.5 mm. The number of cells for computations was varied from 2 to 4.5 million elements. A mesh size of 1.2 mm was considered sufficient to obtain grid-independent results with approximately 3.6 million grid points. The grid convergence was calculated based on the Grid Convergence Index (GCI) criteria. If the GCI for two successive grid sizes was below 3%, it was considered that grid convergence has been achieved [15].

2.2. Reactants dilution ratio (R_{dil})

R_{dil} was calculated at different axial planes of the combustor. For the case of $Q_{th} = 21.5$ kW

($R_C = 0$ mm) with exit port diameter of 25 mm, a maximum R_{dil} of 3.2 was achieved. Complete flameless combustion with low emissions was observed experimentally. R_{dil} was calculated for higher thermal inputs ($Q_{th} = 40.8$, 65.1 and 84.7 kW) with different R_C of 10, 15, 20, 25 and 30 mm and results are shown in Fig. 2. It was observed that, for constant thermal input and increasing R_C, the degree of flow reversal increased in the combustor. The resulting R_{dil} increased with R_C. For instance, at $Q_{th} = 21.5$ kW, a maximum R_{dil} of 5.22, 5.77, 6.26 and 6.75 was obtained for $R_C = 10$, 15, 20 and 25 mm respectively (Fig. 2a). The curved profile of the combustor dome and chamfer near the exit combined to form curved vanes promoted a large degree of flow reversal. Hence, R_{dil} increased with increased R_C. For a constant R_C and increasing thermal input, R_{dil} was calculated as shown in Fig. 2a–d. For example, at $R_C = 25$ mm, the maximum R_{dil} calculated were 6.77, 3.75, 3.51 and 2.71 respectively, for 21.5, 40.8, 65.1 and 84.7 kW. Therefore, it was observed that with increasing thermal input, the chamfer radius must be increased appropriately to maintain a constant R_{dil} for all thermal inputs. The zone length of $R_{dil} > 2.71$, which is the lower limit for achieving flameless combustion is calculated for all computational conditions and shown in Fig. 2e. It was observed experimentally that an $R_C = 20$, 25 and 30 mm were sufficient to achieve flameless combustion at higher heat intensities (10.2, 16.3 and 21.1 MW/m³ respectively).

2.3. Residence time distribution

The residence time of the reactants in the combustion chamber is a significant parameter to achieve flameless combustion [23]. Three basic time parameters were considered to calculate the residence time of reactants.

1. Average residence time; $\tau_{avg} = \left(\frac{V}{\dot{v}}\right)$; $V =$ combustor volume and $\dot{v} =$ volume flow rate of reactants. However, since the present combustor operates with a swirl flow, the residence time was calculated computationally for different cases by injecting particles from air/fuel inlets in the combustor.

2. Swirl based residence time with $R_C = 0$ mm; $\tau_{s(Rc=0mm)}$.

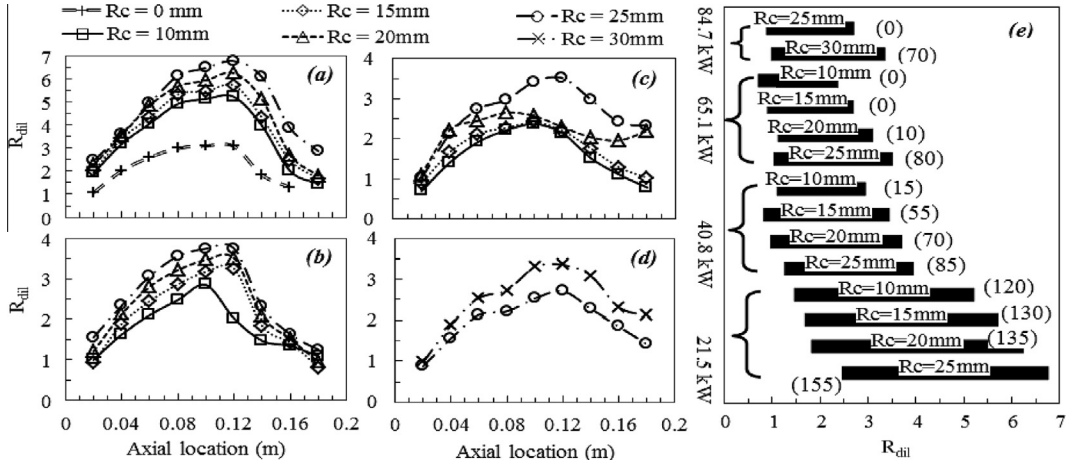Fig. 2. Variation of R_{dil} with R_C (a) 5.37 MW/m^3 (b) 10.2 MW/m^3 (c) 16.3 MW/m^3 (d) 21.1 MW/m^3 (e) Minimum and maximum R_{dil} for all cases and zone length of $R_{dil} > 2.72$ (in parenthesis).

3. Swirl based residence time with $R_C = 25$ mm; $\tau_{s(Rc=25mm)}$.

The calculated τ_{avg} decreased from 0.61 to 0.15 s as the thermal input increased from 5.37 to 21.1 MW/m^3. The calculated $\tau_{s(Rc=0mm)}$ with swirl flow, decreased from 0.76 to 0.29 s and $\tau_{s(Rc=25mm)}$ decreased from 0.98 to 0.69 s for this same range of thermal inputs. For the case of 21.1 MW/m^3, the percentage increase in residence time is 93% and 360% for $\tau_{s(Rc=0mm)}$ and $\tau_{s(Rc=25mm)}$ respectively as compared with τ_{avg}. It was observed from the computational study that the residence time increased with both swirl flow pattern and increased chamfer radius (R_C). Residence time distribution, $E(t)$ [23] was calculated for all cases by considering the combustor as a well-stirred reactor and shown in Fig. 3. The $E(t)$ of the reactor is the probability density function of a particle in the reactor. If $E(t)$ of a reactor is high, the residence time of the particle is large. It is observed from Fig. 3 that $E(t)$ increases with swirl flow, and increases further with chamfer plus swirl flow.

3. Details of experimental methodology

3.1. Experimental setup

Figure 4 shows a schematic diagram of the experimental setup. The combustor was placed vertically on a test stand. Kerosene was stored at a pressure of 9 bar (ΔP) in a pressurized stainless-steel tank. The fuel injector was located at the center of the combustor. The fuel injector imparts a clockwise rotation to fuel spray; hence a counter-clockwise air injection was selected to impart more shear force to the flow resulting in enhanced mixing and evaporation of droplets. Air supply to the combustor was regulated
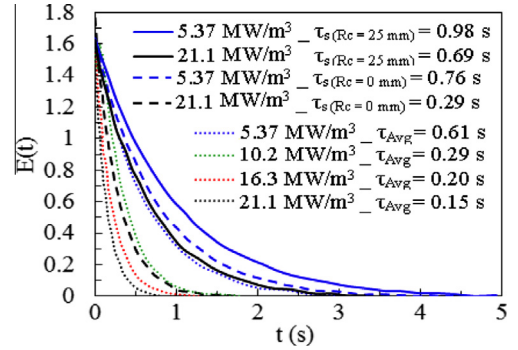

Fig. 3. Residence time distribution ($E(t)$) for three cases based on τ_{avg}, $\tau_{s(Rc=0mm)}$ and $\tau_{s(Rc=25mm)}$.
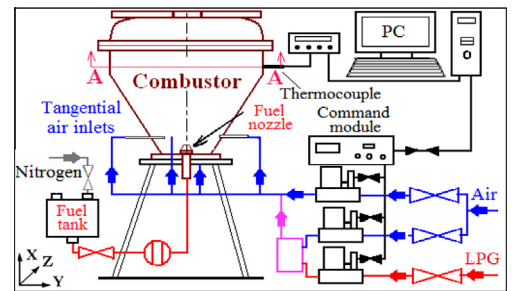

Fig. 4. Schematic diagram of experimental setup.

through electric mass flow controllers (accuracy $\pm 1.5\%$ of full scale).

3.2. Experimental procedure and instruments

Initially, the premixed LPG-air mixture was ignited with a spark and combustor was run for

2–3 min to preheat the combustor. The kerosene fuel is injected at 5 bar pressure by opening the ball-valve in the fuel line. The LPG flow rate was then gradually reduced and the kerosene injection pressure was simultaneously raised to 9 bar. A stable flame was established in conventional combustion mode with stoichiometric kerosene-air mixture for next 4–5 min. After an initial start-up time of 7–8 min, the combustor wall temperature reached ~900 K. A chamfered flange was placed at the top to effectively reduce the exhaust port diameter from 90 mm to a diameter (D) for the particular heat intensity (Table 2). The conventional flame then gradually shifted to a flameless combustion mode. This strategy was adapted to understand and evaluate the effect of exit port diameter variation on transition between conventional (90 mm) and flameless combustion mode (30 mm). The present combustor can be started with the top components in place for a real practical application.

Exhaust gas composition was measured with a gas analyzer which included O_2 analyzer (0–25% range, 0.1% accuracy), CO analyzer (0–10,000 ppm, ±5 ppm accuracy), NO analyzer (0–5000 ppm, ±1 ppm accuracy), CxHy analyzer (0–50,000 ppm), and CO_2 analyzer. Temperature measurements were carried out with R-type ($d_{junction} = 1$ mm) thermocouples. The sound level at the exit (100 mm away from axis) of the combustor was measured for different combustion modes with a fast response (Resolution = 0.1 dB, $\tau_{response} = 200$ ms) sound level instrument.

4. Results and discussion

4.1. Spray characteristics

In the present study, four nozzles N1–N4 with mass flow rates of 1.72, 3.27, 5.21 and 6.78 kg/h respectively, were used to provide 21.5, 40.8, 65.1 and 84.7 kW thermal inputs respectively. An injection pressure of 9 bar was maintained for all experiments. Various details of the spray characteristics such as D_{10}, D_{32} (SMD), D_{V10}, D_{V50} and D_{V90}, droplet distribution, droplet number density (DND) were measured with a particle shadowgraphy technique. 7000–9000 droplets were considered in each sample size. A count of 150 pictures was selected for each sample at an axial position of 45 mm from the nozzle tip.

It was observed that for all four nozzles, SMD was in the range of 35–37 μm and variation in other diameters was relatively very small. Since the spray cone angle and droplet diameters were nearly the same for all four nozzles, the DND increased for higher mass flow nozzles, the measured DND for N1–N4 nozzles was 32×10^3, 64×10^3, 110×10^3 and 167×10^3 n/cm³ respectively. Therefore, entrainment of hot gases needed

to be increased significantly with the increasing DND to achieve complete evaporation of all droplets. The DND distribution for all four nozzles is shown in Fig. 5.

4.2. Temperature distribution

Temperature variation in the radial direction of the combustor at an axial location of 120 mm was measured for different heat intensities at $\Phi = 0.92$ and comparison with predicted results is shown in Fig. 6. Due to larger thermocouple response time (~0.25 s) as compared to integral turbulence time-scales (~3 ms), it is difficult to measure actual temperature variation in the combustor. However, temperature variation with time is measured at a given location and the mean was calculated from recorded temperatures over a period of 10–20 s. The measured temperature was corrected by considering convection and radiation losses from the thermocouple junction. For the case of 5.37 MW/m³, the wall temperature of the combustor was ~800 K. When the combustor was operated at 10.2 MW/m³, the walls became red hot. Hence, cooling of outer walls of the combustor was mandatory for higher heat densities, achieved through water circulation through copper tubes brazed on the outer walls of the combustor. A constant wall temperature of ~950 K was maintained for higher heat intensities (10.2–21.1 MW/m³). The heat removal through wall cooling is 3.2, 8.3, and 12.9 kW respectively for three higher heat intensities of 10.2, 16.3 and 21.1 MW/m³. Fresh air at ambient temperature entered the combustor and circulated on the inner walls; a sharp rise in temperature of the air was observed near the walls of the combustor (Fig. 6). Temperature at all radial locations increased with increasing heat intensity of the combustor. As expected, the temperature increased from the walls to the center line of the combustor. The temperature difference across the plane, from axis to near wall (0.0975 m) for 5.37 MW/m³ with $R_C = 0$ mm was 443 K. The temperature difference for higher heat intensities
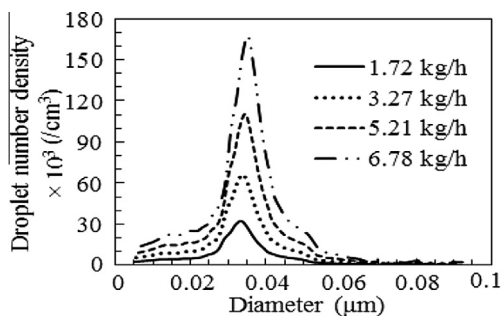

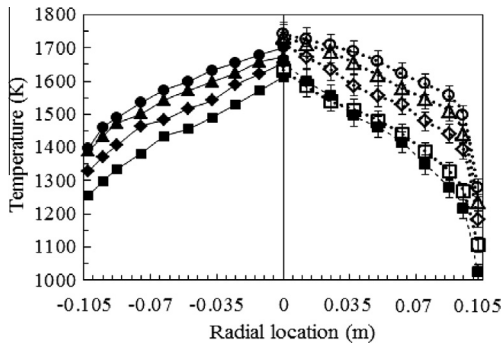Fig. 5. Distribution of DND for nozzles of different fuel flow rates.

Fig. 6. Temperature distribution comparison of experimental and computational measurements (– ■ – 5.37 MW/m^3_R_C = 0 ⋅■⋅ 5.37 MW/m^3_R_C = 20 ⋅◇⋅ 10.2 MW/m^3_R_C = 25 ⋅▲⋅ 16.3 MW/m^3_R_C = 25 ⋅●⋅ 21.1 MW/m^3_R_C = 30 ■ 5.37 MW/m^3_R_C = 20_Comp ◆ 10.2 MW/m^3_R_C = 25_Comp ▲ 16.3 MW/m^3_R_C = 25_Comp ● 21.1 MW/m^3_R_C = 30_Comp.

(10.2–21.1 MW/m^3) was 319, 293 and 245 K respectively. With increased heat intensity, the overall temperature of the combustor and the temperature of the fresh air circulating increased. Hence the temperature gradient across the radial direction decreased significantly. Maximum temperature at the center of the combustor increased from 1633 to 1741 K as heat intensity increased from 5.37 to 21.1 MW/m^3. The temperature fluctuations around the mean value were in the range of 1.3–1.8% for all cases (variation bands shown in Fig. 6). A low temperature gradient and smaller fluctuations are representative characteristics of flameless combustion. For all thermal input conditions, the maximum temperature is below 1800 K. Therefore, NO$_x$ emissions were expected to be relatively very low. The predicted temperatures in the central zone are slightly lower than the measured temperatures for all thermal inputs. For the outer region (next to the central zone), the predicted temperatures are slightly higher than measured temperatures. Uniformly distributed temperature with low temperature gradients is observed in computational studies.

4.3. Pollutant emissions

The CO, NO$_x$ and HC emissions were measured for the range of operating conditions and emission levels were corrected to 15% O$_2$ level and shown in Fig. 7. CO emissions increased with a decrease in Φ from 1 to 0.6 and increase in heat intensity. However, the specific emissions index (ppm/kW) decreased with increasing heat intensity. For R_C = 20 mm and $\dot{Q}'''$=5.37, 21.1 MW/m^3, CO emissions varied from 11 to 21 ppm and 25 to 41 ppm respectively, as Φ varied from 1 to

0.6. The specific CO emissions for these cases varied from 0.51 to 0.977 ppm/kW and 0.3–0.48 ppm/kW respectively. The emission release rate decreased with increasing heat intensity, indicating a positive outcome for higher heat density combustion systems. NO$_x$ emissions decreased with decreasing Φ, as expected. For lean mixtures, the average measured temperature in the combustor decreased with a decrease in Φ. This led to a reduction in the NO$_x$ emissions, however, CO emissions increase slightly. For the case of R_C = 20 mm and $\dot{Q}'''$=5.37, 21.1 MW/m^3, NO$_x$ varied from 9 to 6 ppm and 19–12 ppm respectively, for Φ varied from 1 to 0.6. The specific NO$_x$ emissions for these cases varied from 0.42 to 0.28 ppm/kW and 0.22–0.14 ppm/kW respectively.

HC emissions increased with decreasing Φ from 1 to 0.6 and the specific emissions decreased with increasing heat intensity. For the case of R_C = 20 mm and $\dot{Q}'''$=5.37, 21.1 MW/m^3, HC emissions varied from 0 to 3 ppm and 3–9 ppm respectively, for Φ = 1–0.6. The specific HC emissions for these cases varied from 0 to 0.14 ppm/kW and 0.03–0.1 ppm/kW respectively. The overall variation of CO, NO$_x$ and HC emissions for all heat intensities (Φ = 1–0.6) were measured to be 11–41, 6–19 and 0–9 ppm respectively. These emissions are well within the range of emissions from flameless combustion with gaseous fuels reported in the literature.

A combustor with a chamfer radius of R_C = 25 mm is tested for all thermal inputs (21.5–84.7 kW) conditions. Flameless combustion mode is observed for all cases without any issues related to combustion stability. Minimum recirculation required for each case of thermal input is determined experimentally and computationally by varying from R_C = 10–30 mm.

4.4. Acoustic emissions

Figure 8 shows the variation of acoustic emissions of the combustor in various combustion modes. Base level acoustic emissions of 84 dB were measured initially for cold flow conditions. After ignition, initially the combustor operated in the conventional mode with exit diameter of 90 mm and the level of acoustic emissions increased to an average value of 102 dB. After 3 min of conventional combustion, the chamfered portion was mounted and the exit diameter was reduced to D mm (Table 2). Immediately after reducing the diameter, the sound level increased. After a time of 2–3 min, the swirl flow was well stabilized in the combustor and flameless combustion was observed. The sound level reduced dramatically to a level well below the conventional combustion mode. For the case of 21.1 MW/m^3, 113.5 and 93.6 dB of sound level was observed in the transition and flameless modes respectively. It was observed that with increased heat intensity,
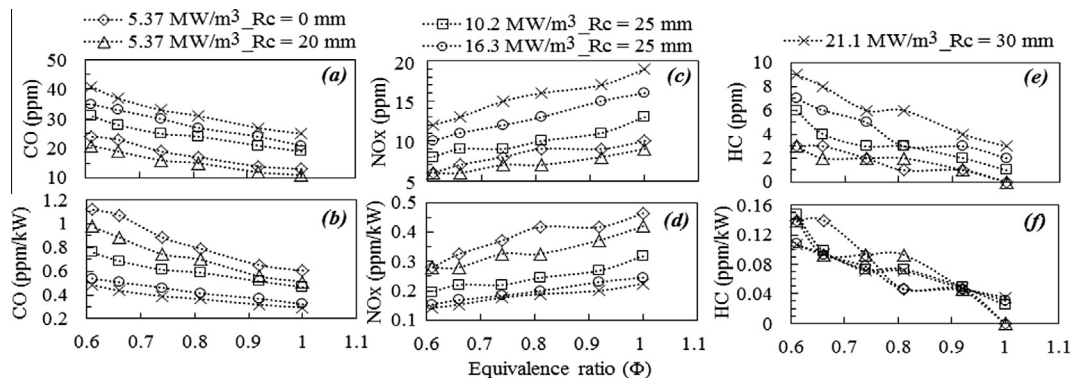
Fig. 7. Variation of emissions with equivalence ratio for different heat intensities.
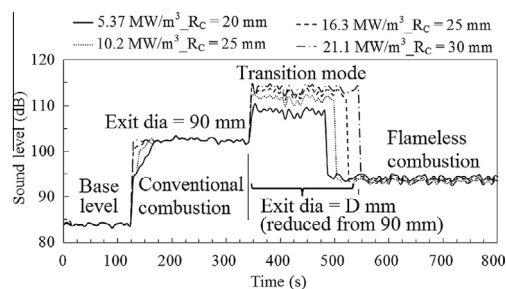

Fig. 8. Variation of acoustic emissions for all heat intensities.

the sound level increased during the operation of the combustor in transition mode. However, for all heat intensities, almost a same sound level of approximately 94 dB was observed during the flameless combustion mode. The overall net sound level reduction from conventional to flameless mode for all combustors was in the range of 8–9 dB. A similar reduction has been reported in the literature [7,14].

5. Conclusions

In the present work, a new combustor configuration was designed and scaled-up to achieve flameless combustion with liquid fuels at high heat intensities for various industrial and gas turbine applications. Observations are summarized below.

1. Flameless combustion was stabilized in the base combustor with 21.5 kW thermal input (5.37 MW/m^3) and maximum R_{dill} of 3.2 with very low emissions. However, flameless combustion was not achieved and unburned fuel accumulated in the combustor for higher fuel flow rates.
2. A chamfer added near the exit in the modified combustor configuration helped increase the R_{dill} and residence time, permitting flameless combustion at higher intensities. The curved

profile of the combustor dome and chamfer combined to form a curved vane which helps increase the degree of flow reversal. A computational investigation with experimental evidence suggests that a chamfer radius of 20, 25 and 30 mm was sufficient to achieve flameless combustion for $\dot{Q}'''=10.2$, 16.3 and 21.1 MW/m^3, respectively.
3. The peak temperature increases in the combustor and the temperature gradients decreases with an increase in the heat intensities. The temperature fluctuations were very small (1.3–1.8% of the mean value) for all cases.
4. The overall variation of CO, NO$_x$ and HC emissions for all heat intensities ($\Phi = 1$–0.6) were 11–41, 6–19 and 0–9 ppm respectively. These emissions are well within the range of emissions from flameless combustion with gaseous fuels operating at high intensity in the literature. Specific emissions (ppm/kW) decrease with an increase in heat intensity.
5. The outstanding performance of the burner with very low chemical and acoustic emissions at high heat release rates indicate the potential for use in various industrial and gas turbine applications.

References

[1] J.A. Wunning, J.G. Wunning, *Prog. Energy Combust. Sci.* 23 (1) (1997) 81–94.
[2] S. Kumar, P.J. Paul, H.S. Mukunda, *Proc. Combust. Inst.* 29 (2002) 1131–1137.
[3] R. Weber, J.P. Smart, W.Vd. Kamp, *Proc. Combust. Inst.* 30 (2005) 2623–2629.

[4] A. Cavaliere, M. de Joannon, *Prog. Energy Combust. Sci.* 30 (4) (2004) 329–366.

[5] M. Derudi, R. Rota, *Proc. Combust. Inst.* 33 (2011) 3325–3332.

[6] G.G. Szego, B.B. Dally, G.J. Nathan, *Combust. Flame* 156 (9) (2009) 429–438.

[7] S. Kumar, P.J. Paul, H.S. Mukunda, *Proc. Combust. Inst.* 30 (2005) 2613–2621.

[8] V.K. Arghode, A.K. Gupta, *Appl. Energy* 111 (2013) 930–956.

[9] J. Mi, P. Li, B.B. Dally, R.A. Craig, *Energy Fuels* 23 (11) (2009) 5349–5356.

[10] R.A. Yetter, I. Glassman, H.C. Gabler, *Proc. Combust. Inst.* 28 (2000) 1265–1272.

[11] R. Lückerath, M. Meier, M. Aigner, *ASME J. Eng. Gas Turbines Power.* 130 (2008) 011505.

[12] R. Weber, *Proc. Combust. Inst.* 26 (1996) 3343–3354.

[13] M.D. Bohon, W.L. Roberts, *Proc. Combust. Inst.* 34 (2013) 1705–1712.

[14] V.M. Reddy, D. Sawant, D. Trivedi, S. Kumar, *Proc. Combust. Inst.* 34 (2013) 3319–3326.

[15] V.M. Reddy, P. Garg, P. Biswas, S. Kumar, *Fuel Process. Technol.* 118 (2014) 310–317.

[16] V.M. Reddy, Flameless Combustion with Liquid Fuels, Ph.D. Thesis, Indian Institute of Technology Bombay, India, 2013.

[17] C. Syred, W. Fick, A.J. Griffiths, N. Syred, *Fuel* 83 (17–18) (2004) 2381–2392.

[18] A.E.E. Khalil, A.K. Gupta, *Appl. Energy* 88 (11) (2011) 3685–3693.

[19] K.K.J.R. Dinesh, K.W. Jenkins, M.P. Kirkpatrick, W. Malalasekera, *Combust. Sci. Technol.* 184 (5) (2012) 629–659.

[20] Y.M. Al-abdeli, A.R. Masri, *Combust. Sci. Tech.* 179 (1–2) (2007) 207–225.

[21] V.M. Reddy, D. Trivedi, D. Sawant, S. Kumar, *Combust. Sci. Tech.* (in preparation).

[22] D.B. Spalding, *Proc. Combust. Inst.* 9 (1963) 833–843.

[23] J.M. Beer, K.B. Lee, *Proc. Combust. Inst.* 10 (1965) 1187–1202.